



# Computational Investigation of the Effects of Chemistry on Mars Retropropulsion Environments

**Jan-Renee Carlson**

**Bill Jones**

**Ashley Korzun**

**Gabriel Nastac**

**Eric Nielsen**

**Aaron Walden**

**Li Wang**

*NASA Langley Research Center*

**Pat Moran**

**Tim Sandstrom**

*NASA Ames Research Center*

**Paul Kolano**

*Inu Teq, LLC*

**Alexander Kuhn**

**Justin Luitjens**

**Jörg Mensmann**

**Marc Nienhaus**

**Dragos Tatulea**

**Rajko Yasui-Schoeffel**

*NVIDIA Corp.*

**Christopher Stone**

*National Institute of Aerospace*

**Mohammad Zubair**

*Old Dominion University*











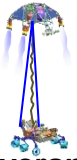

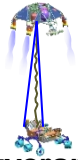
This research used resources of the Oak Ridge Leadership Computing Facility at the Oak Ridge National Laboratory, which is supported by the Office of Science of the U.S. Department of Energy under Contract No. DE-AC05-00OR22725.



# Retropropulsion for Human Mars Exploration

## Human-scale Mars landers require new approaches to all phases of Entry, Descent, and Landing

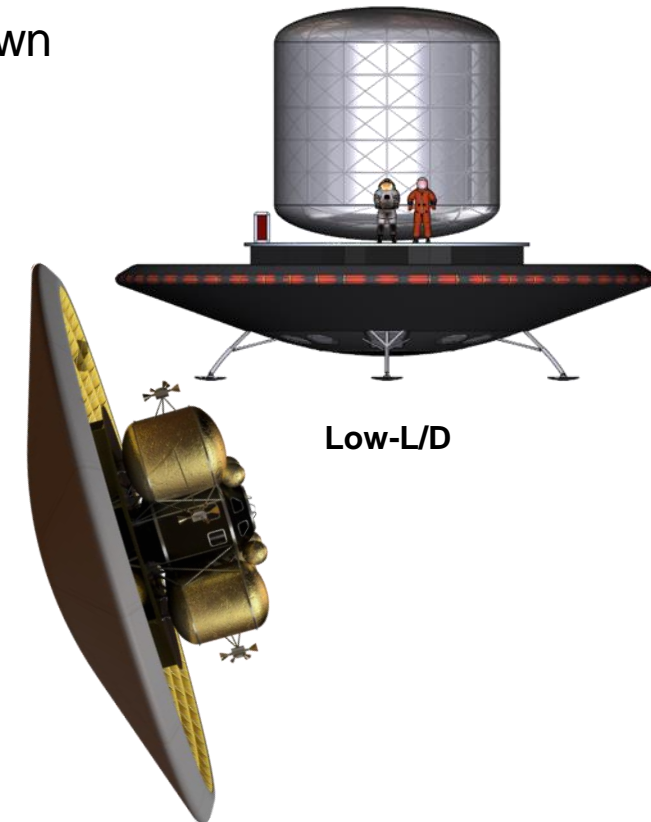
- Cannot use heritage, low-L/D rigid capsules → deployable hypersonic decelerators or mid-L/D rigid aeroshells
- Cannot use parachutes → retropropulsion, from supersonic conditions to touchdown
- No viable alternative to an extended, retropropulsive phase of flight

	Viking	Pathfinder	MERs	Phoenix	MSL	InSight	M2020
Entry Capsule (to scale)							
Diameter (m)	3.505	2.65	2.65	2.65	4.52	2.65	4.5
Entry Mass (t)	0.930	0.584	0.832	0.573	3.153	0.608	3.440
Parachute Diameter (m)	16.0	12.5	14.0	11.8	19.7	11.8	21.5
Parachute Deploy (Mach)	1.1	1.57	1.77	1.65	1.75	1.66	1.75
Landed Mass (t)	0.603	0.360	0.539	0.364	0.899	0.375	1.050
Landing Altitude (km)	-3.5	-2.5	-1.4	-4.1	-4.4	-2.6	-2.5
Landing Technology	 Retro- propulsion	 Airbags	 Airbags	 Retro- propulsion	 Skycrane	 Retro- propulsion	 Skycrane

### Human-Scale Lander (Projected)

16 - 19  
40 - 65  
N/A  
N/A  
26 - 36  
+/- 2.0

Retro-  
propulsion



Steady progression of “in family” EDL

New EDL Paradigm



# Governing Equations and FUN3D Background

- Conservation of species, momentum, energies, and turbulence variables
- Two-temperature model available for thermal nonequilibrium
- Variable species, energies, and turbulence equations
- Node-based finite-volume approach on general unstructured grids
- Fully implicit formulation is used to integrate the equations in time
  - Block sparse linear system  $\mathbf{Ax}=\mathbf{b}$
  - Matrix  $\mathbf{A}$  composed of diagonal and off-diagonal  $N_{eq} \times N_{eq}$  blocks
  - Memory and solution time increases as  $O(N_{eq}^2)$
- System solved with multicolor point-implicit approach

$$\begin{aligned}\frac{\partial}{\partial t}(\rho y_s) + \frac{\partial}{\partial x_j}(\rho y_s u_j) - \frac{\partial}{\partial x_j}(J_{sj}) &= \dot{\omega}_s \\ \frac{\partial}{\partial t}(\rho u_i) + \frac{\partial}{\partial x_j}(\rho u_i u_j + p \delta_{ij}) - \frac{\partial}{\partial x_j}(\tau_{ij}) &= 0 \\ \frac{\partial}{\partial t}(\rho E) + \frac{\partial}{\partial x_j}((\rho E + p)u_j) - \frac{\partial}{\partial x_j}\left(u_k \tau_{kj} + \dot{q}_j + \sum_{s=1}^{N_s} h_s J_{sj}\right) &= 0 \\ \frac{\partial}{\partial t}(\rho E_v) + \frac{\partial}{\partial x_j}(\rho E_v u_j) - \frac{\partial}{\partial x_j}\left(\dot{q}_{vj} + \sum_{s=1}^{N_s} h_{vs} J_{sj}\right) &= S_v \\ \frac{\partial}{\partial t}(\rho \tilde{v}) + \frac{\partial}{\partial x_j}(\rho \tilde{v} u_j) - \frac{\partial}{\partial x_j}\left(\frac{1}{\sigma}\left(\mu \frac{\partial \tilde{v}}{\partial x_j} + \sqrt{\rho} \tilde{v} \frac{\partial \sqrt{\rho} \tilde{v}}{\partial x_j}\right)\right) &= S_{\tilde{v}}\end{aligned}$$

$$\mathbf{q} = [\rho \vec{y}_s, \rho \vec{u}, \rho E, \rho E_v, \rho \tilde{v}]^T$$

$$\int_V \frac{\partial \mathbf{q}}{\partial t} dV + \oint_S (\mathbf{F} \cdot \mathbf{n}) dS - \int_V \mathbf{S} dV = \mathbf{0}$$

$$\left[ \frac{V}{\Delta \tau} \mathbf{I} + \frac{V}{\Delta t} \mathbf{I} + \frac{\partial \hat{\mathbf{R}}}{\partial \mathbf{q}} \right] \Delta \mathbf{q} = -\mathbf{R}(\mathbf{q}^{n+1,m}) - \frac{V}{\Delta t} (\mathbf{q}^{n+1,m} - \mathbf{q}^n)$$

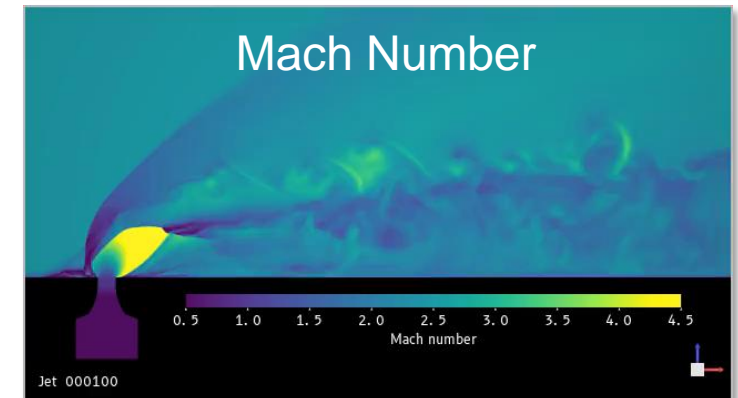
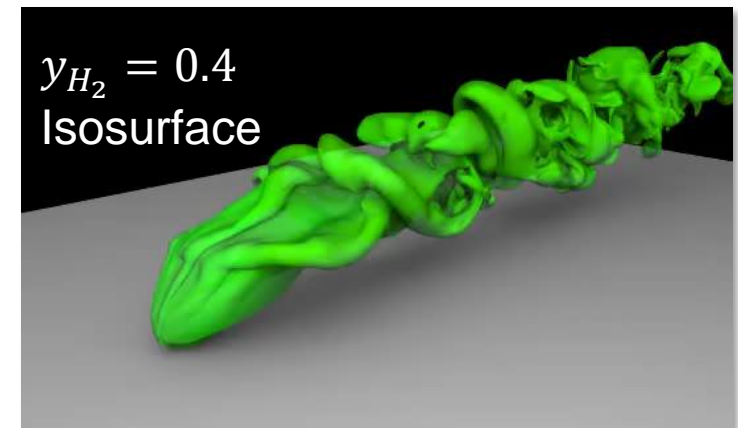
$$\mathbf{q}^{n+1,m} = \mathbf{q}^{n+1,m} + \Delta \mathbf{q}$$



# GPU Implementation

- FLUDA library
  - CUDA C++ port of compute kernels in FUN3D
  - No external libraries required
  - Use of library in FUN3D is controlled by a run-time parameter
- Pre-processing routines remain on the host
- All PDE kernels (~150) performed on the device
- Minimal data transfer between host/device (mainly scalars)
  - Large data motion only at user-specified frequencies (e.g., restarts, visualization support)
- Data structures are identical between CUDA and Fortran contexts
  - Column-major order array layouts
  - GPU “mirror” data structures that match CPU data structures
  - Variable precision is identical to CPU approach
    - FP64 for most variables, with mixed FP16/FP32/FP64 for linear algebra

## Transverse Hydrogen Jet in Supersonic Cross Flow: $M_\infty = 2.4$ , 9 species, DES







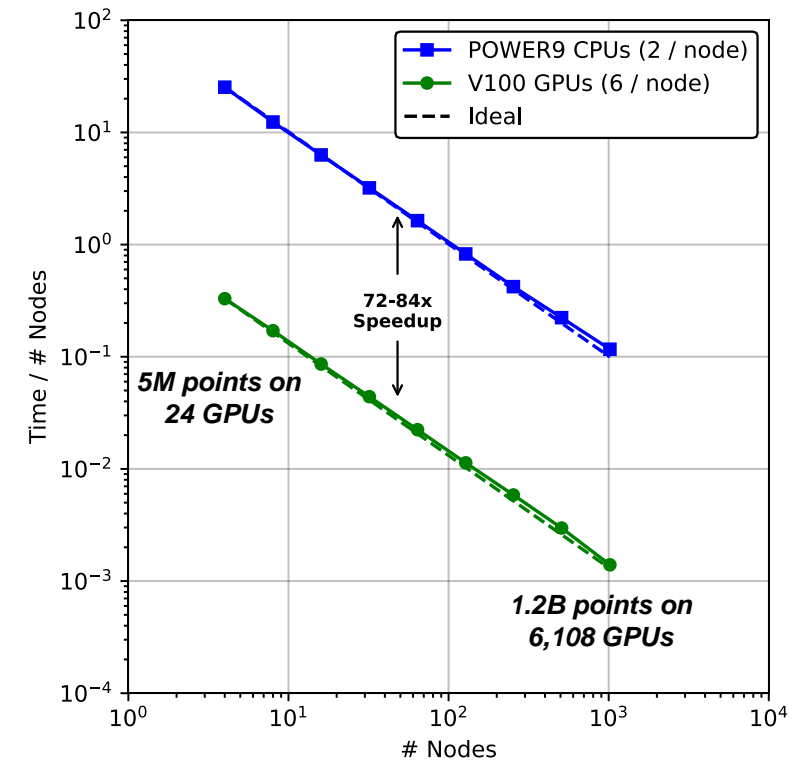
# Optimizations and Performance

- Reduction of kernel state
  - Initial naive CUDA port resulted in stack frames so large that GPU ran out of memory immediately
  - To remedy, multiple threads are assigned to a work item, which reduces 2D arrays to scalars in many cases
  - Strategic use of registers, shared memory
- Reduce thread divergence
- Coalesced memory accesses
- Kernel launch parameter optimization via auto-tuning framework
- Shared-memory transposition, pre-atomic warp aggregation to minimize collisions
  - SC21 IA<sup>3</sup> paper: Stone, C., et al., “*Accelerating Unstructured-Grid CFD Algorithms on NVIDIA and AMD GPUs*”
- B-SpMV benefits from prefetching, asynchronous copies directly from HBM (A100), vector persistence in L2 (A100)
  - SC21 MCHPC paper: Zubair, M., et al., “*Memory Optimizations for Sparse Linear Algebra on GPU Hardware*”

## Device-Level Performance (13s/1e/2t)

2 x 64-core AMD 7742	1.0x
NVIDIA V100 32 GB	4.0x
NVIDIA A100 40 GB	7.0x

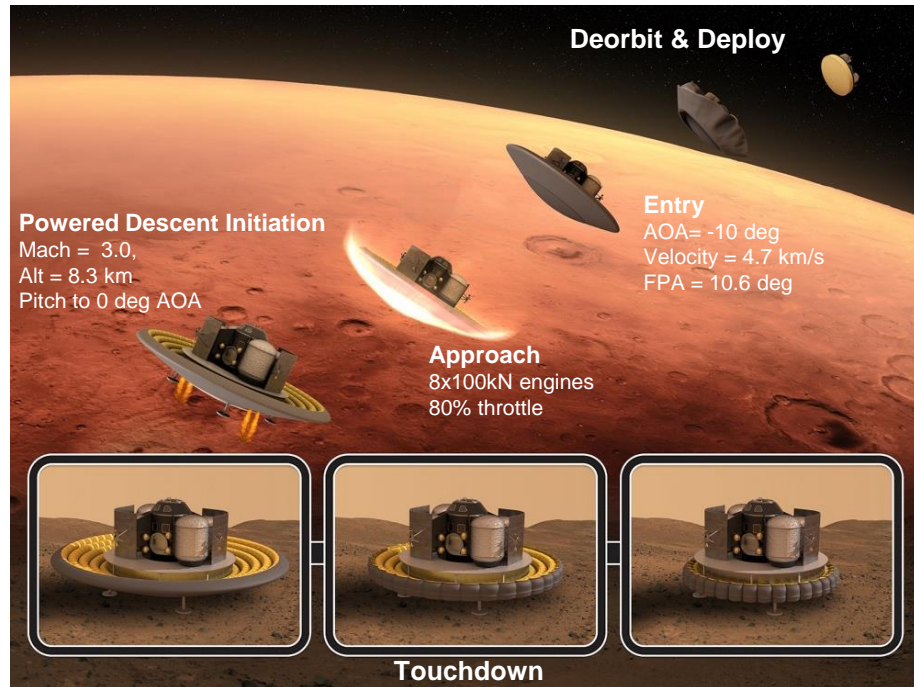
## Scaling on Summit





# Early Science 2018, INCITE 2019/2021 Efforts

## “Aero-Propulsive Real Gas Effects for Human-Scale Mars Entry”



Previous campaigns focused on perfect gas simulations

- Limited experiments on Earth are perfect gas

Current efforts are exploring effects of reacting-gas chemistry on these retropropulsion flows across the flight trajectory

- Methane combustion in Martian  $\text{CO}_2$  atmosphere
- ~10x more expensive computationally
- All work completed on Summit, enabling full-scale simulations encompassing several seconds of physical time in a few days
- Each simulation uses thousands of GPUs, equivalent to several million CPU cores

### Campaign Goals

- **Science**: Advance the understanding of retropropulsion flow physics during Mars EDL of a human-scale lander
- **Computational**: Demonstrate production readiness and efficiency advantages of GPU implementation of FUN3D at scale



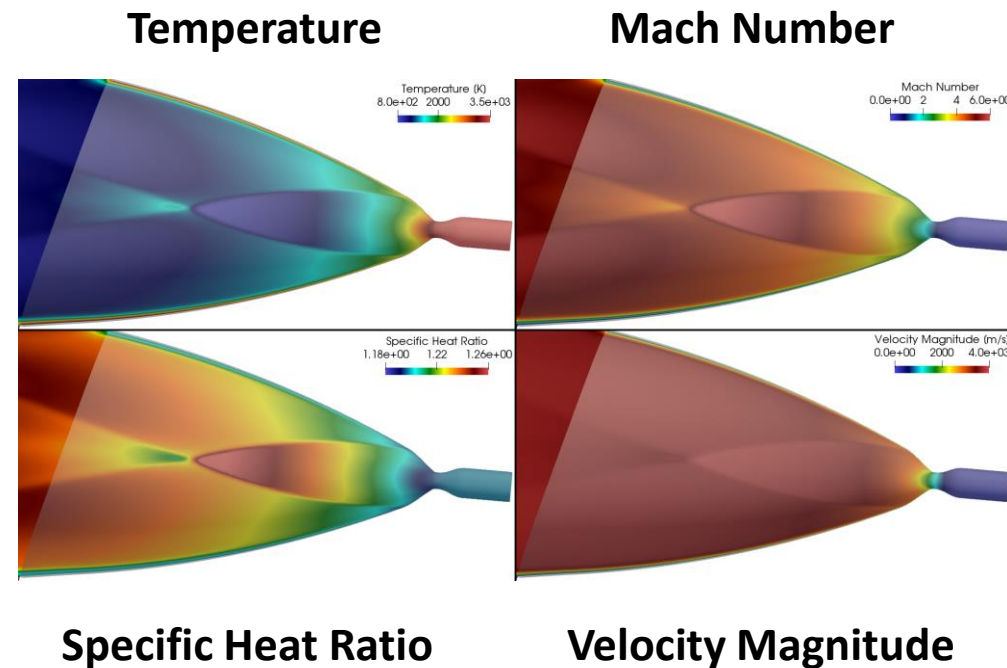
# Simulation Overview

## Physical Modeling

- $M_\infty = 2.4 / 1.4 / 0.8$ ;  $Re_D = 5.9M / 4.6M / 3.0M$
- Martian atmosphere (97% CO<sub>2</sub>, 3% N<sub>2</sub> by mass)
- 8 engine plena set equilibrium composition of the products of methane-oxygen combustion
  - O/F = 3.5 with  $T_0 = 3582$  K,  $p_0$  based on throttle setting
- 10-species, 19-reaction mechanism
- Nozzle area ratio = 177
  - Boundary layer at nozzle exit ~8% of nozzle exit radius
- Detached Eddy Simulation based on SA-Catris model
- All walls modeled as no-slip

## Computational Approach

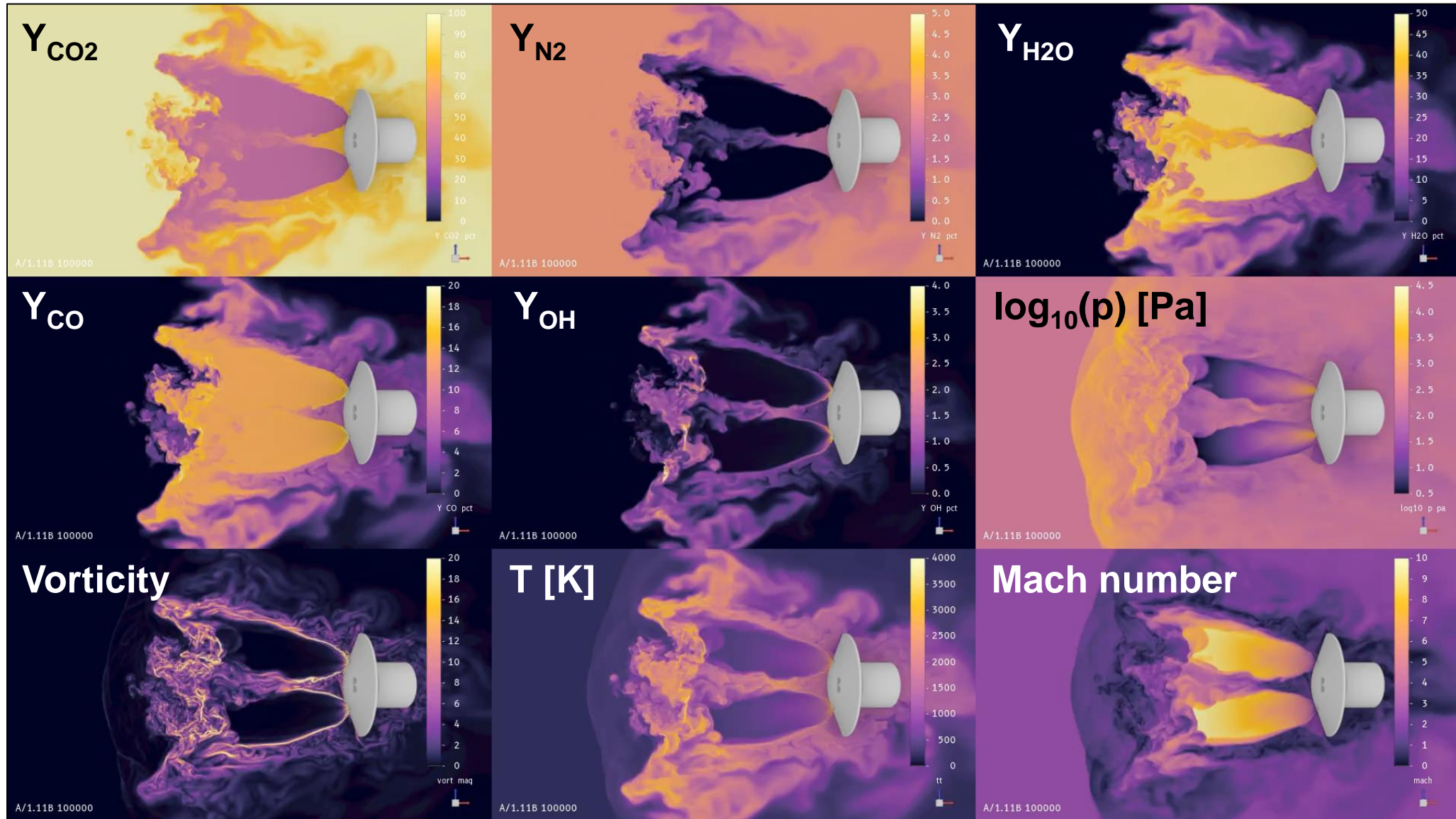
- Spatial mesh: ~6B elements / ~1.3B points
- 300K-500K timesteps (5 subiterations), with total integration time of ~2-4 seconds
- Running up to 2,652 nodes on Summit (15,912 V100s)
- I/O: storing 20 variables per grid point (~90 GB) every ~30 seconds for entire 2-day simulation
  - Parallel asynchronous I/O, less than 1% overhead
  - ~1 PB per simulation, migrating about ~50 TB/day from DOE to NASA







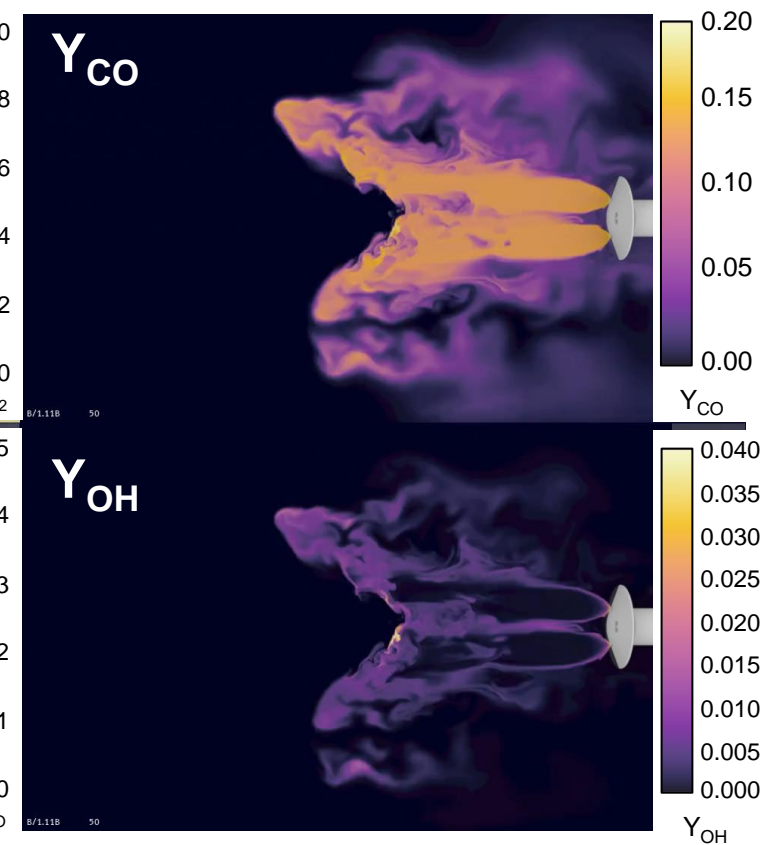
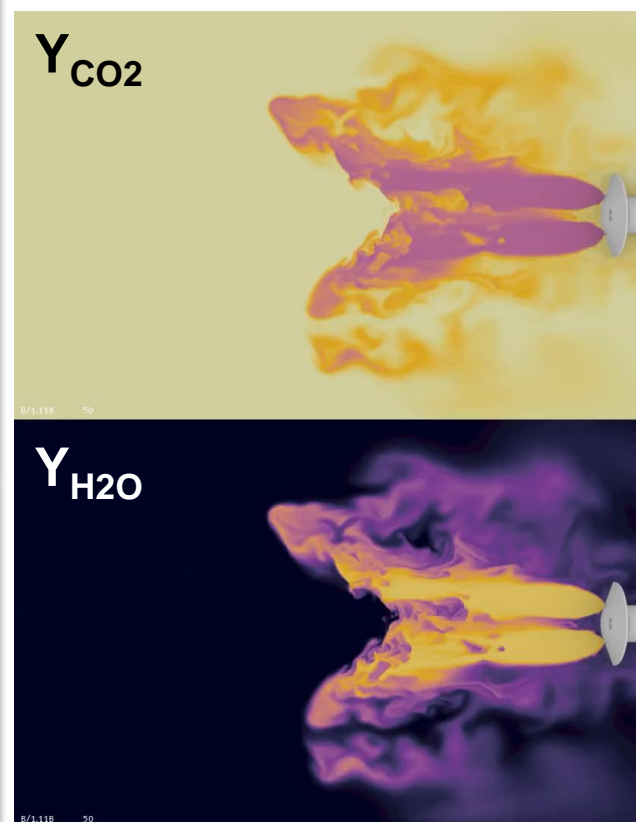
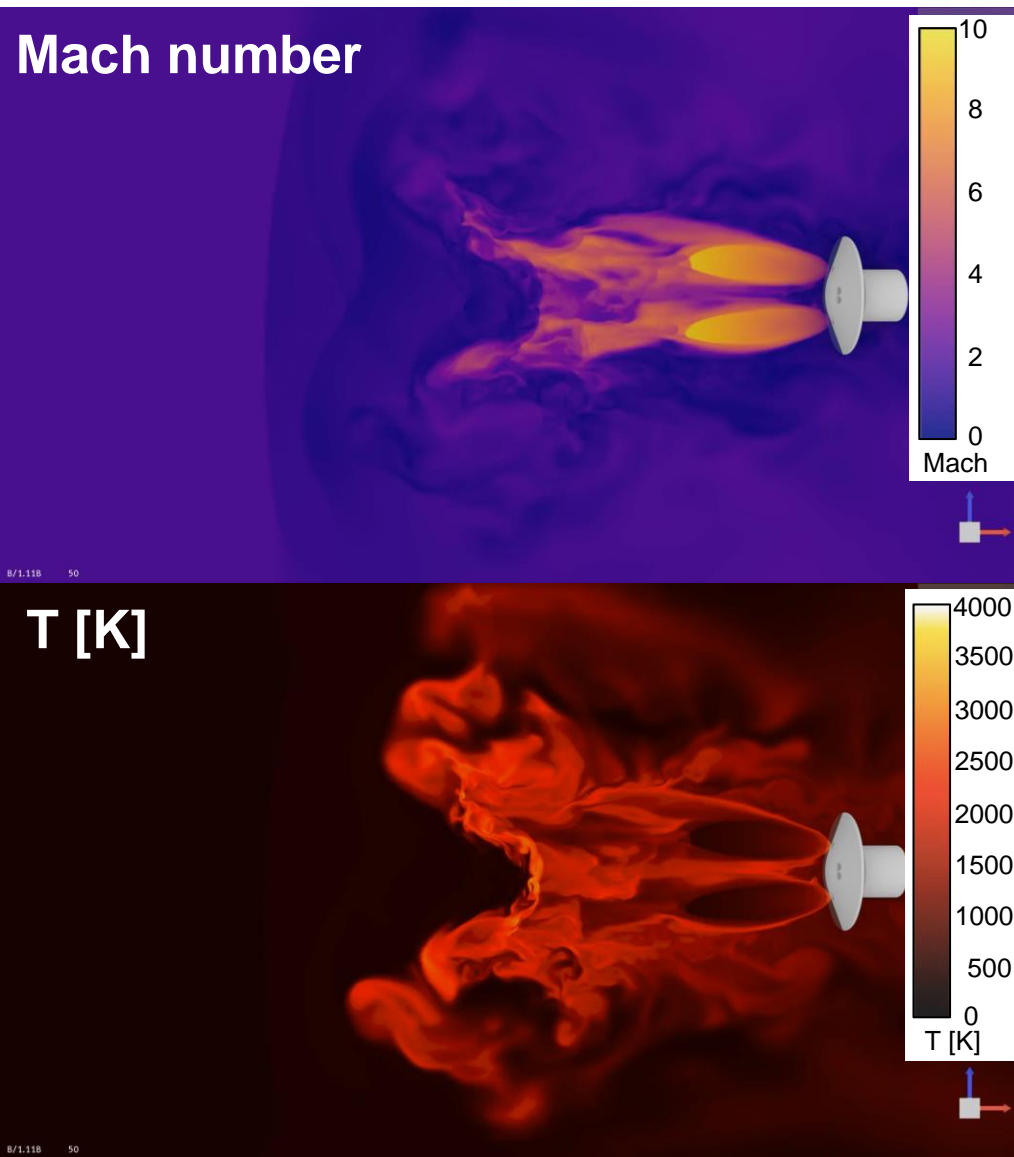
# *Supersonic Results ( $M_\infty = 2.4$ )*





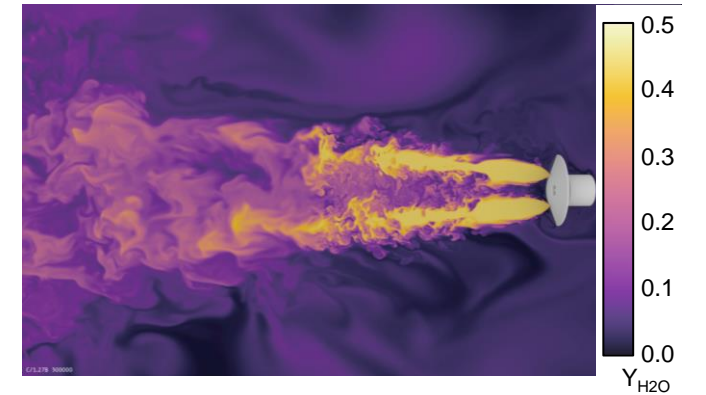
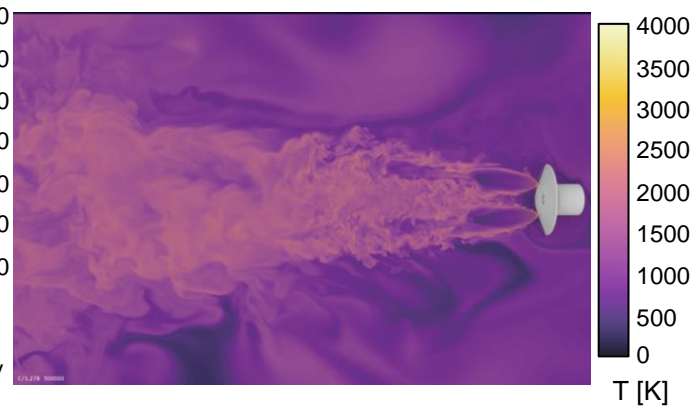
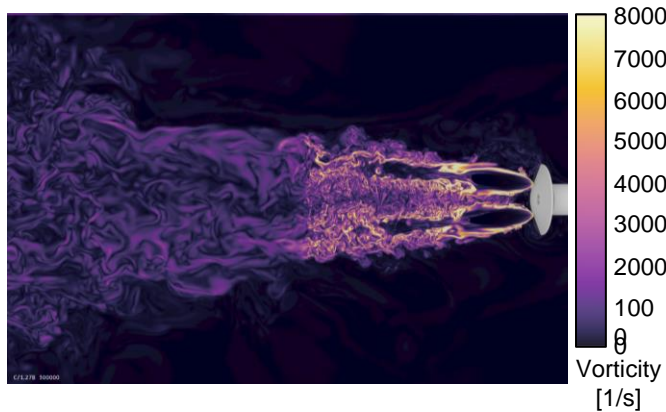
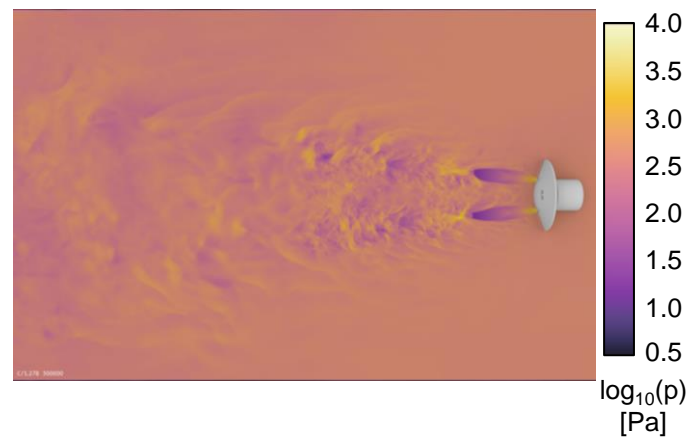
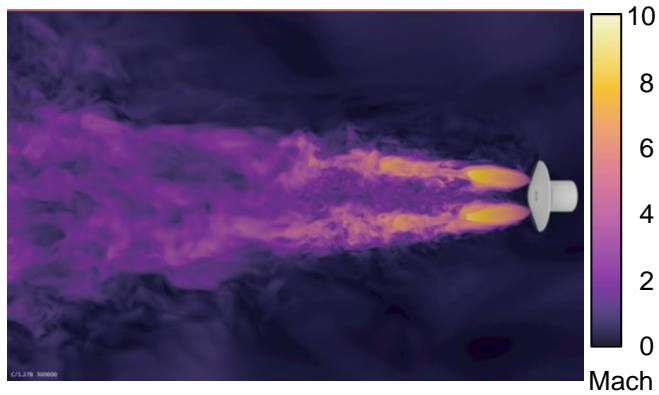


# Transonic Results ( $M_\infty = 1.4$ )





# *Subsonic Results ( $M_\infty = 0.8$ )*

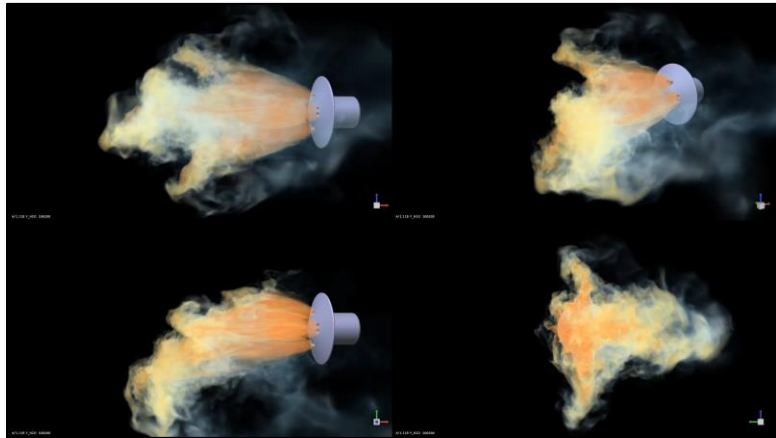


Instantaneous Flowfield Quantities

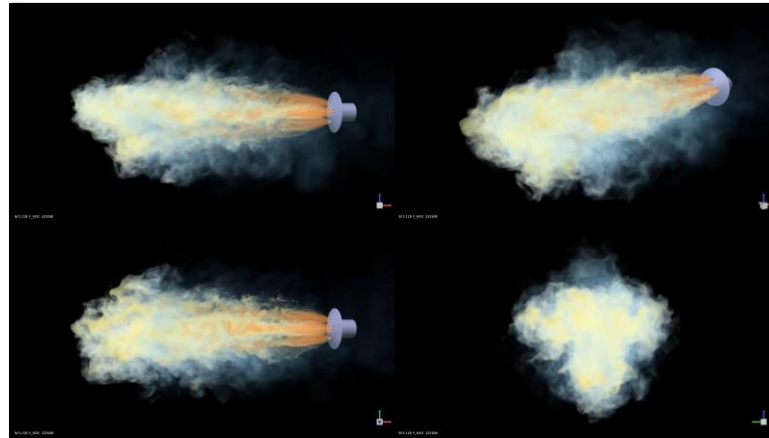


# Visualization Across All Conditions

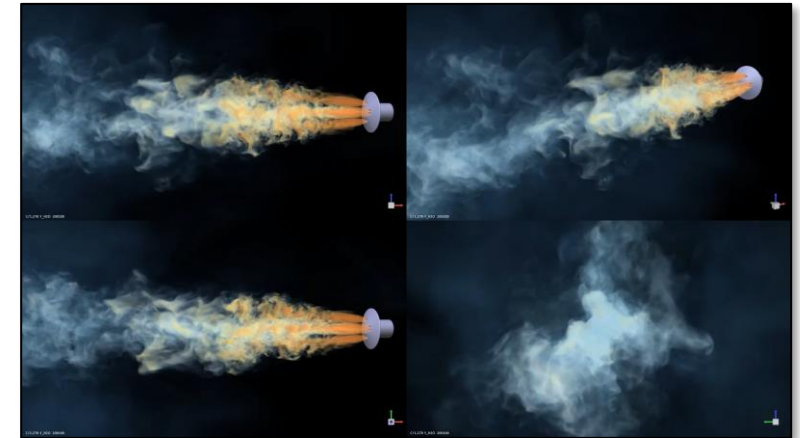
$M_\infty = 2.4$



$M_\infty = 1.4$

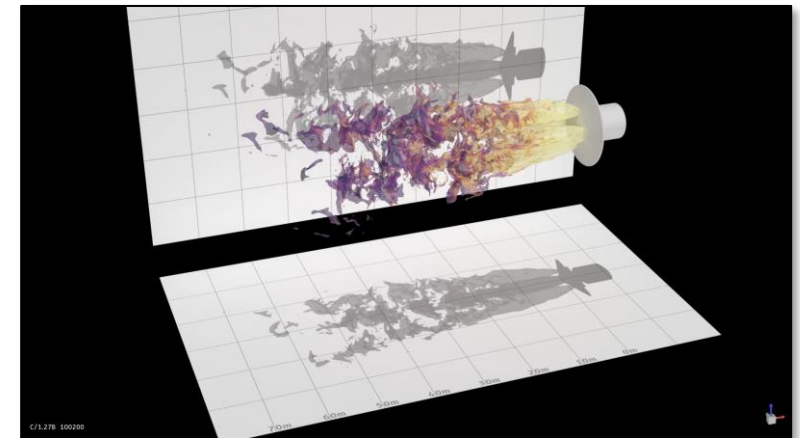
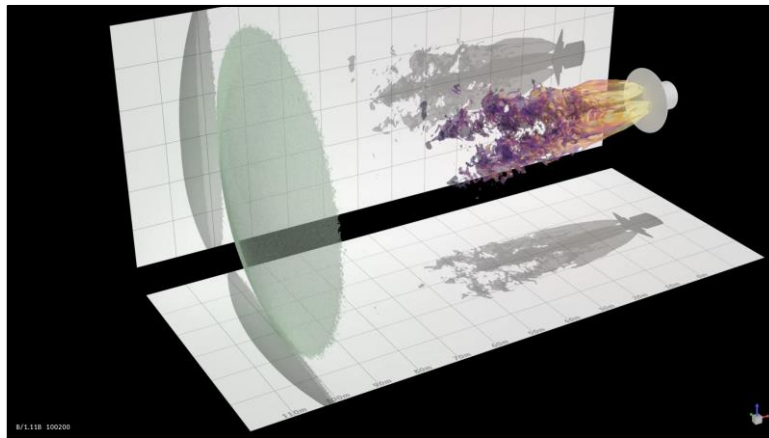
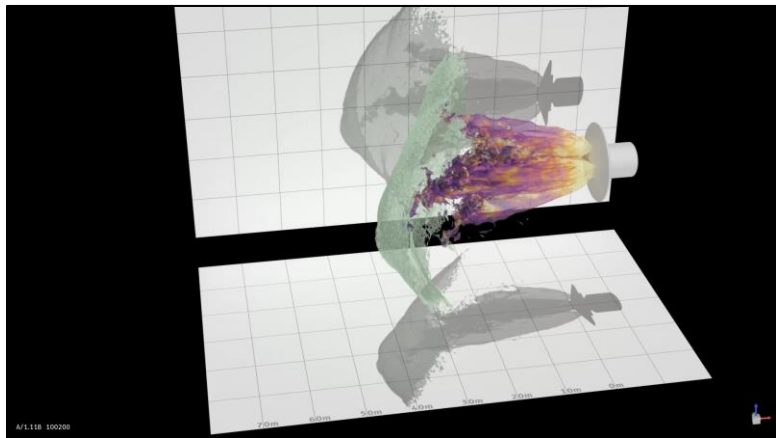


$M_\infty = 0.8$



Volume Renderings of  $\text{H}_2\text{O}$  Produced by NVIDIA IndexX

0.00 0.45



Shock with Isosurfaces of  $Y_{\text{H}_2\text{O}} = 0.40$ , Colored by Vorticity Magnitude

(each Cartesian grid line represents 10 meters)





# *Impacts of Chemistry*

- Dynamic similarity is maintained for key parameters such as freestream Mach number, Reynolds number, nozzle exit-to-stagnation freestream pressure ratios, nozzle exit Mach number, and dynamic pressure
- Primary difference is incorporation of chemistry
- Flow structures for chemically-reacting simulations are qualitatively similar to perfect gas air simulations
  - Throttling conditions investigated behave similarly
- Engine thrust accounts for the majority of the axial force on the vehicle for both gas models
- Key differences include:
  - Specific heat ratio varies substantially in the nozzles and upstream of the vehicle due to strong temperature dependence of carbon dioxide and other species
  - Significant minor species concentrations including hydroxyl radical (~4%) upstream of the vehicle potentially impacting thermal design
  - Reacting-gas simulations predict larger (40%+) aerodynamic axial forces compared to perfect gas air



# *Summary*

- Full-scale wall-resolved, chemically-reacting CFD simulations have been performed for a conceptual human-scale Mars lander with retropropulsion at supersonic, transonic, and subsonic flight conditions
- All work performed on Summit system located at Oak Ridge National Laboratory
- Consistent with subscale experiments and past simulations, the aerodynamic contribution to total deceleration force during powered descent is small ( $< 6\%$  due to aerodynamics)
- Significant minor species concentrations are present upstream of the vehicle ( $Y_{OH} > 4\%$ ), and the specific heat ratio varies greatly both in the nozzles ( $1.19 \leq \gamma \leq 1.26$ ) and upstream of the vehicle



*Thank you for having us!*